Check for updates

Self-propelled bioglass janus nanomotors for dentin hypersensitivity treatment†

Wei Wu, [iD]^c Hang Chi,[c] Qianyang Zhang,[c] Ce Zheng,[e] Narisu Hu,*[a,c] Yingjie Wu [iD] *[d] and Jiaxin Liu*[b]

Dentin hypersensitivity treatment is not always successful owing to the exfoliation of the blocking layer. Therefore, efficiently delivering a desensitization agent into the dental tubule is critical. Nanomotors are widely used as *in vivo* drug delivery systems owing to their strong power and good biocompatibility. Herein, we report a kind of self-propelled bioglass Janus nanomotor with a Pt motion unit (nBGs@Pt) for application in dentin hypersensitivity that was prepared *via* a simple sol−gel method and magnetron sputtering method, with an average size of 290 nm. The Pt layer as the power unit provided the dynamics to deliver the bioglass (desensitization agent). Using hydrogen peroxide as a fuel, the nBGs@Pt could automatically move in different media. In addition, the nBGs@Pt with a mesoporous structure demonstrated good hydroxyapatite formation performance. An *in vitro* dentin pressure model was used to verify the blocking ability of the nBGs@Pt in dentin tubules. The dynamics of the nBGs@Pt was sufficient to resist the outflow of dentin fluid and movement into the dentin tubules, with a blocking rate of 58.05%. After remineralization, the blocking rate could reach 96.07% and the formation of hydroxyapatite of up to 10 µm or more occurred. It is expected that this study will provide a simple and feasible new strategy for the painless treatment of dentin sensitivity.

1. Introduction

Dentin hypersensitivity (DH) is a common dental problem that affects many people. The hydrodynamic theory explains the severe pain in dentin sensitivity.[1] Because of exposed dentinal tubules, any stimulation, such as temperature, mechanical, and chemical stimulation, will often increase the fluid flow within the dentinal tubules, leading to short-term severe pain.[2] So far, blocking the exposed dentin tubules with a desensitization agent is an effective way to prevent stimulation.[3] In general, an ideal desensitization agent should be able to produce long-term stable minerals that can effectively block the interior of dentinal tubules and form a mineralized layer on their surface.[4] Until now, several excellent desensitiz-

ing agents have been invented and have proven to have good blocking abilities.[5] Among them, bioactive glasses have shown good biological activity[6−8] and are widely used as dental materials.[9−11] Compared with conventional (micrometer-sized) bioactive glasses, the nanoscale offers a wider range of applications in bone substitution, dental applications, and bone tissue engineering.[12] Radial mesoporous bioactive glasses show good hydroxyapatite (HA)-forming ability owing to their radial mesoporous structure and high specific surface area,[13] which allow them to serve as a blocking layer to cut-off stimulation. However, the blocking layer is above the surface, instead of going into the dentin tubule, and so the therapeutic effect always eventually fails, and the tooth sensitization resumes due to daily tooth brushing or chewing.[14] So a method to efficiently deliver bioactive glasses into the dental tubule is critical.

Nanomotors as a micro-scale power device can convert other forms of energy into kinetic energy, making the particles move autonomically.[15−20] The unique physical properties and different driving strategies of nanomotors allow them to perform multiple tasks, such as anti-bacteria, environmental interactions, opening cell membranes, or delivering drugs *in vivo* precisely.[21−27] Compared with other types of nanomotors, chemically driven nanomotors have lower weight, a higher thrust-to-weight ratio, and lower energy consumption and are thus widely used in a wide range of applications.[28]

^a*Oral Implant Centre, The Second Affiliated Hospital of Harbin Medical University, Harbin 150086, People's Republic of China. E-mail: hmuhunarisu@163.com*
^b*Department of Pharmaceutics, School of Pharmacy, Harbin Medical University, Harbin, 150086, People's Republic of China*
^c*Hard Tissue Development and Regeneration Laboratory, Harbin Medical University, Harbin, 150086, People's Republic of China*
^d*School of Medicine and Health, Harbin Institute of Technology, Harbin, 150001, People's Republic of China*
^e*Hospital Management Office of Harbin Medical University, Harbin, 150086, People's Republic of China*
†Electronic supplementary information (ESI) available. See DOI: https://doi.org/10.1039/d3nr03685e

Pt is often used as the power unit of chemical-driven nanomotors owing to its stable chemical properties and high catalytic efficiency.[29] Hydrogen peroxide (H_2O_2), a platinum catalytic substrate fuel, is currently widely used as a flushing solution for dental treatment.[30,31] Based on this, we developed a kind of nanomotor that uses H_2O_2 as fuel. Nanomotors are expected to deliver bioactive glasses into dentin tubules and seal them from the inside, thus avoiding stripping of the surface-blocking layer to maintain the long-term efficacy as an efficient drug carrier.

Herein, we chose nano radial mesoporous bioactive glasses (nBGs) prepared by a modified sol–gel method as the core, applied single-sided Pt asymmetric modification *via* magnetron sputtering as the power units, and successfully prepared self-actuating hydroxyapatite (HA)-forming mesoporous Janus nanomotors (nBGs@Pt), as shown in Scheme 1. We first investigated the morphology, size, zeta potential, and objective images of the nanomotors, and then respectively studied the motion behaviors of the nanomotors under different conditions and their biosafety to human gingival fibroblasts or mice. Finally, *in vitro* dentin disks were utilized to study the treatment effectiveness.

2. Materials and methods
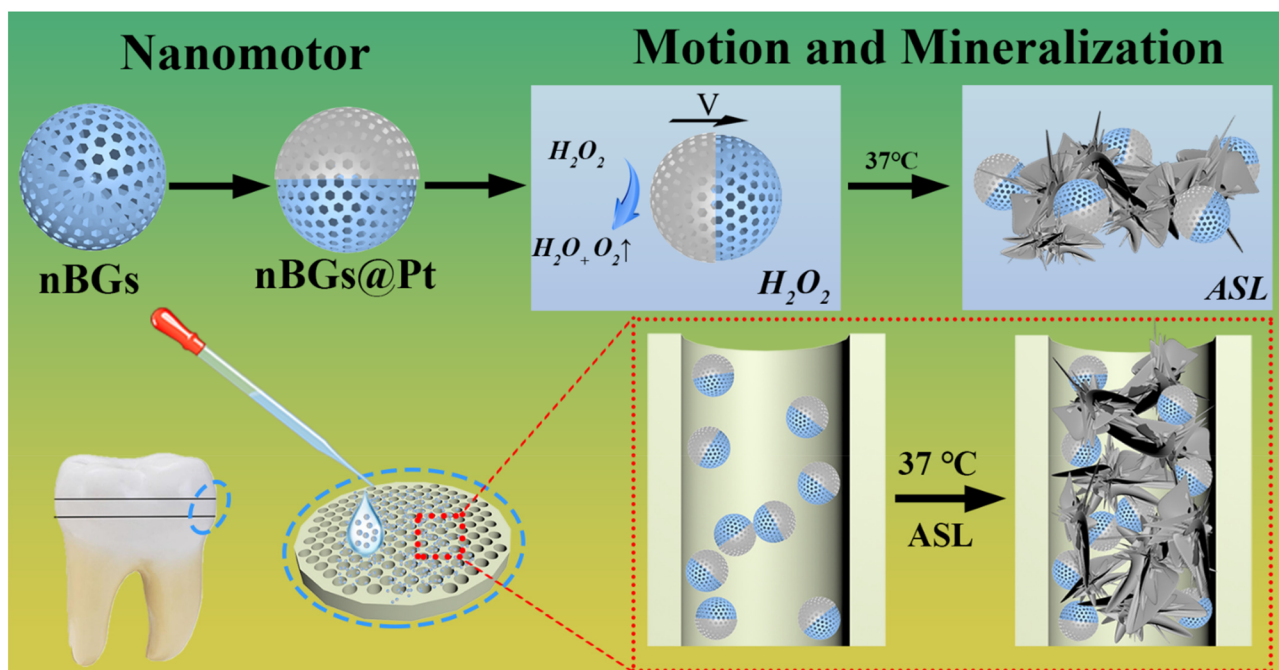
2.1 Materials

Cetyltrimethylammonium tosylate (CTA·Tos, ≥99%), 1-butyl-3-methylimidazolium triuoromethanesulfonate ([BMIM] OTF),

triethanolamine (TEA, ≥99%), tetraethyl orthosilicate (TEOS, ≥99%), triethyl phosphate (TEP, ≥99%), calcium nitrate tetrahydrate (CN, ≥99%), and doxorubicin (DOX, ≥99%), were purchased from MACKLIN, Shanghai. Polycarbonate films were purchased from Safelab, Beijing. Artificial saliva (ASL), Ringer's solution, and Cell Counting Kit-8 (CCK-8) were purchased from Phygene, Fuzhou. Human gingival fibroblasts (HGFs) were purchased from ATCC. The teeth were obtained from the Second Affiliated Hospital of Harbin Medical University and their use was approved by the Medical Ethics Committee (YJSKY2022-384). All laboratory animals were purchased from the Animal Experiment Center of the Second Affiliated Hospital of Harbin Medical University and their use was approved by the Animal Ethics Committee of the Harbin Medical University, Harbin, China.

2.2 Synthesis of the nBGs@Pt

The nBGs were synthesized using our improved method in accordance with the reported method.[32] With CTA·Tos as a surfactant, [BMIM] OTF ionic liquid as a cosurfactant, TEA as a mineralizing agent, water as a solvent, TEOS as a silicon source, TEP as a phosphorus source, and CN as a calcium source, monodispersed nBGs with center-radial large pores were prepared by the sol–gel method.

Briefly, a mixture of 0.96 g CTA·Tos, 0.3 g [BMIM] OTF, 0.105 g TEA, and 50 mL water was strongly stirred at 80 °C for 1 h to form a surfactant solution. Subsequently, 7.29 g TEOS was quickly added to the surfactant solution. The above

Scheme 1 Self-propelled bioglass Janus nanomotors composed of a body (bioglass) and power unit (Pt layer). With the addition of fuel, the Pt layer catalyzes hydrogen peroxide decomposition and generates power by forming differential concentration on both sides of the Janus nanomotor. The mesoporous structure provides a large specific surface area to make the nanomotor form HA rapidly. The motors are sent to the dentinal tubule and can penetrate in-depth and then form HA as a blocking layer.

mixture was stirred at 80 °C at a speed of 1000 rpm for 2 h at 80 °C. Then, 0.1 g TEP was quickly added into the mixture with stirring at a speed of 1000 rpm for another 1 h. The white precipitate was collected by centrifugation, washed 3 times alternately with ethanol and water, and then dried in the air at 60 °C overnight. Next, an appropriate amount of CN was dissolved in 5 mL ethanol, and the above dried white powder was then added into the CN solution and then shaken for up for 24 h. After natural drying, the above powder was placed in a Muffle furnace and calcined in the air at 650 °C for 3 h. Finally, the white powder was redispersed with ethanol and stored at 4 °C for future use.

The prepared nBGs were uniformly dispersed on the glass sheet to form a monolayer of particles. Platinum was coated on the exposed side by a magnetron vacuum sputtering instrument (QUORUM Q150R Plus) at a pressure of 2.5 mTorr and a power of 200 W. The Janus particles were collected by ultrasonic treatment and washing alternately with water and ethanol three times. After drying in air at 60 °C, the obtained nBGs@Pt was stored in ethanol at 4 °C for future use.

2.3 Characterization of the nBGs@Pt

An appropriate amount of nBGs@Pt in ethanol was dispersed on a silicon slice and carbon film. Scanning electron microscopy (SEM, HITACHI SU5000) at 20 kV and transmission electron microscopy (TEM, ThermoFisher Scientific Talos200X S) at 200 kV were used to observe the morphology of the particles. Energy dispersive X-ray spectroscopy (EDS, HITACHI SU5000) was used to determine the distribution of elements. Laser particle size analysis (Zetasizer Lab, Malvern) was performed to measure the mean particle size and zeta potential. The particles were analyzed by X-ray diffraction (XRD, PANalytical B.V. X'Pert PRO).

2.4 Motion analysis of the nBGs@Pt

An appropriate amount of nBGs@Pt was ultrasonically dispersed in water. The dispersion and the fuel (1 : 1) were added to the surface of the slides together, and the nBGs@Pt trajectory was observed with an inverted optical microscope (OLYMPUS IX71) and recorded at the same time. The trajectories of the nBGs@Pt in different concentrations of fuel H_2O_2 (1%, 3%, 5%, w/v) with the same water medium and nBGs@Pt in 3% H_2O_2 fuel with different media (ASL and Ringer's solution) were observed. ImageJ was used to analyze the movement trajectory in 3 s (random 30 particles) and then the time-MSD curve was drawn based on a previous research method.[33]

The diffusion coefficient was measured using a laser particle size analyzer (Zetasizer Lab, Malvern). The nBGs@Pt dispersion was configured in a suitable concentration, and then diluted with H_2O_2 to 3% using H_2O, ASL, and Ringer's solution respectively. Next, an appropriate amount of fuel was taken for the sample pool according to the manufacturer's instructions, and then an appropriate amount of dispersion was added into the fuel (no bubbles in the sample pool). The diffusion coefficients of nBGs@Pt in water (no fuel), with different concentrations of fuel (1% H_2O_2, 3% H_2O_2, 5%

H_2O_2), and different media (ASL and Ringer's solution) with fuel of 3% H_2O_2 were separately measured. The measurements were repeated 10 times and the average was taken to draw the image.

2.5 In vitro toxicity tests

The cell lines were incubated at 37 °C under an atmosphere of 5% CO_2. HGFs were selected to detect the in vitro cytotoxicity of nBGs@Pt using the CCK-8 kit. HGFs (100 μL per well) were inoculated in 96-well plates and cultured for 24 h. Then, 10 μL of nBGs@Pt with different concentrations (1, 0.5, 0.25, 0.125, and 0.1 mg mL^{-1}) or normal saline were added and incubated at 37 °C for 48 h, and then 10 μL CCK-8 solution was added to each well. After incubation for 3 h, the absorbance (450 nm) of each group was detected to calculate the cell viability.

2.6 In vivo toxicity tests

Female BALB/c mice (4–6 weeks old) were selected to test the toxicity of nBGs@Pt. A total of 12 mice were randomly divided into the nBGs@Pt group and the control group. The mice in the nBGs@Pt group were given the nBGs@Pt dispersion by gavage for 3 consecutive days, while the mice in the control group were given normal saline. After administration, the mice were weighed for 10 d, then the arterial blood was collected for routine blood examination. The mice were sacrificed after collecting the blood. The main organs (heart, liver, spleen, lung, and kidney) were collected and hematoxylin and eosin staining (H&E) was performed on them.

2.7 Ex vivo dentin tubule blocking experiments

An appropriate amount of nBGs@Pt in ASL was taken in 3 cuvettes, respectively, with the fresh ASL renewed every 24 h. The particles were collected by centrifugation respectively at 1, 4, and 7 d and then washed 3 times with water and ethanol and then dried. The final product was observed by SEM and analyzed by XRD.

The isolated dentin disks were prepared according to the reported method,[34,35] in which freshly extracted maxillary third molars aged 20–40 years old were selected, disinfected after scraping off the soft tissue, soaked in normal saline, and stored at 4 °C. The excess dental tissue was removed with a grinding wheel and 2 mm thick dentin disks were formed. The disks were stored at 4 °C in normal saline after EDTA etching.

The dentin tubule was filled with dentin fluid, which was constantly drained due to the presence of pressure in the pulp cavity. To construct the in vitro dentin pressure model in our study, Ringer's solution was used to simulate the dentin fluid and the pressure of the pulp cavity was simulated by hydraulic pressure (controlled by adjusting the distance between the fluid level and the dentin disk to a height of 27 cm), according to previous studies.[36,37] Each dentin disk was fixed on the polymer cover and all the sides were sealed with wax to make sure no liquid flowed except on the surface of the dental disk. Before the experiments, each fixed dentin disk was soaked in Ringer's solution and vacuumed for 20 min to make sure the disks were filled with liquid.

The nBGs@Pt or nBGs were ultrasonically dispersed in water, respectively. Then, 10 μL dispersion was added and 10 μL fuel in the dentin disk pressure model and kept under that condition for 10 min, which was recorded as 1 treatment. Then, the dentin disk was removed, gently brushed with a toothbrush 10 times, and then rinsed alternately with ethanol and water three times. The same method was adopted to treat the dentin disk pressure model three times. The SEM images of the dentin disks from the nBGs group and nBGs@Pt group after 1 or 3 treatments were randomly taken. If a single dentin tubule was blocked by more than 50%, it was recorded as a blocking success. As long as it was noted that particles were entering into the dentin tubules, it was considered an entry success. The blocking rate and entry rate were calculated according to the images.

2.8 *In vitro* dentin mineralization experiments

The dentin disks that had been treated three times by nBGs@Pt in "Section 2.7" were recovered and incubated with ASL at 37 °C. The immersion solution was changed every 24 h. After 7 d incubation, the surface morphology of the dentin disks was observed by SEM, and then the sample was carefully broken to avoid contamination of the fractured side, and the longitudinal section of HA formation was observed by SEM.

2.9 Statistical analysis

All data are expressed herein as the mean ± standard deviation (S.D.). A one-way analysis of variance followed by the *t*-test was applied in all the statistical comparisons.

3. Results and discussion

3.1 Synthesis and characterization of the nBGs@Pt

The nBGs@Pt was prepared as shown in Fig. 1a. Fig. S1† shows the characteristic of the nBGs. The TEM image (Fig. 1b) shows that the nBGs@Pt was spherical and arborescent with a radial large mesoporous structure. This structure provides a large specific surface area, which can accelerate HA formation. A typical nBGs@Pt Janus nanomotor particle is shown in Fig. 1c, where it can be seen that after precious metal deposition, the Pt-coated layer at the higher left part is brighter, prompting the Janus structure. The EDX image (Fig. 1d) showed that the Pt element was highly concentrated in the higher left part of the particles, confirming the successful Pt deposition. Fig. 1e shows the size distribution of the nBGs@Pt, with the greatest spread being around 290 nm. The diameter of the nanoparticles observed in the SEM images was in accord with the size measured by laser size analysis. Fig. 1f shows the zeta-potential change before and after precious metal deposition. The zeta potential of the nBGs was −10.7 mV and for nBGs@Pt was −12.91 mV, showing the existence of the Pt layer led to a slight potential decrease. That means Pt was successfully incorporated. There was a SiO_2 peak (amorphous phase) at 20°–30°, while the characteristic peaks of Pt appeared at 40°, 46°, and 68°(PDF#01-071-3756) in the

XRD spectrum (Fig. 1g). These results confirm that we had successfully prepared nBGs@Pt with a Janus structure.

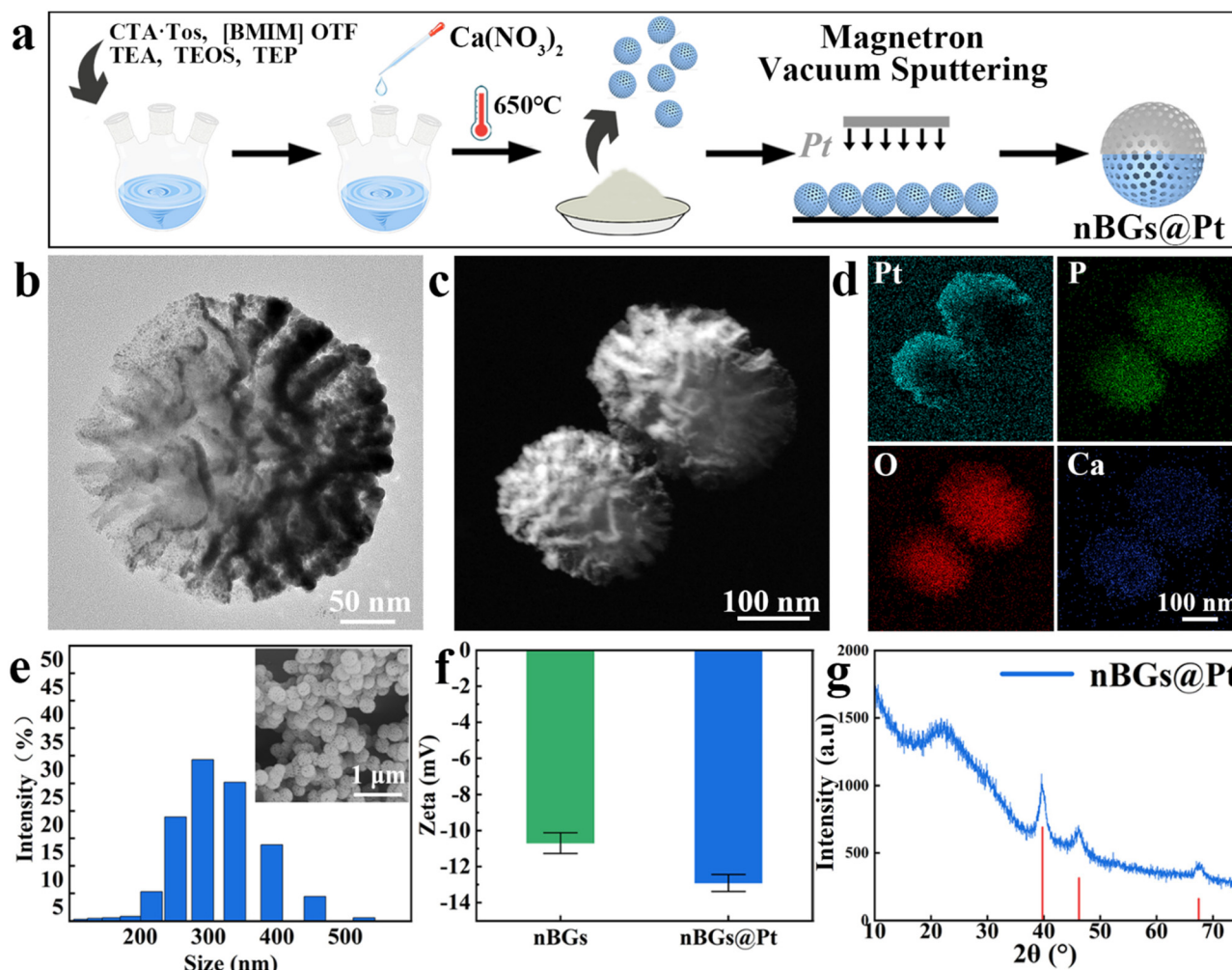### 3.2 Analysis of the motion behaviors of the nBGs@Pt

Based on the Pt on one side of the nanomotors, H_2O_2 was decomposed catalytically into H_2O and O_2, which could also convert chemical energy into kinetic energy. Fig. 2a shows the theory of the nBGs@Pt movement. Here, Pt as a catalyst promotes H_2O_2 decomposition, so the concentration of H_2O_2 at this side decreases and then produces a concentration difference, so the surrounding solution flows here and generates a relative motion with nBGs@Pt, pushing the nBGs@Pt forward.

The motion ability of the nBGs@Pt under different media and different concentrations of fuel were investigated. Fig. 2b shows the typical trajectory under different circumstances in 3 s. We replotted these trajectories and compared them (Fig. 2c). When the medium was water, with the increase concentration (1%–5%) of the additional fuel (H_2O_2), the path of nBGs@Pt was continuously lengthened. Meanwhile, the nBGs@Pt also could move automatically a long way in ASL and Ringer's solution as the medium with 3% H_2O_2. A motion video of all the nanomotors shown in Fig. 2b and c was recorded, see Videos S1 and 2.†

The mean square displacement (MSD) in Fig. 2d confirmed the autonomous motion ability of the nBGs@Pt. The squared displacement was linear over time without fuel, which proved that the nBGs@Pt underwent Brownian motion in water, which is consistent with previous research.[33] When the fuel was added, the curve was parabolic, indicating that the nanomotors moved spontaneously, and the diffusion coefficient also increased with the increase in the fuel concentration (Fig. 2e). Under the condition of 5% H_2O_2 and 3% H_2O_2 as fuel, the curve was obviously parabolic. When 1% H_2O_2 was used as fuel, the curve was relatively smooth, but the nanomotors could still move automatically. Although adding 5% H_2O_2 demonstrated a good motion capacity, it is important to consider that H_2O_2 with a high concentration can damage oral tissue if used incorrectly, and so we chose 3% H_2O_2 for the further fuel tests. Also, 3% H_2O_2 is already widely used as a flushing solution in dentistry. We used the same method to further investigate particle motion in a simulated oral environment by selecting ASL and Ringer's solution as the medium (3% H_2O_2 as fuel), respectively. The curve was a parabola, meaning the nBGs@Pt were still moving automatically in ASL and Ringer's solution. The viscosity of ASL was higher than Ringer's solution, so the path length of ASL was shorter, and also for MSD. The diffusion coefficient also indicated there was an increase in motion. Dentin fluid was continuously discharged at a rate of 0.35 μL min^{-1} cm^{-2} in the absence of external stimulation.[38] We assumed that the diameter of each dentin tubule was 3 μm. Then we calculated the fluid flow rate in a single dentin tubule ($v = Q/S$, where Q is the rate of flow and S is the cross-sectional area), and found the fluid flow rate was 0.0583 μm s^{-1}, much lower than the flow rate measured in Ringer's fluid (1.0561 μm s^{-1} from MSD). We suppose that when the nBGs@Pt enter the dentin tubule, the decrease in

Fig. 1 The preparation and characterization of the nBGs@Pt Janus nanomotor. (a) The preparation process image of the nBGs@Pt. (b) The bright field TEM image of the nBGs@Pt. (c) The dark field TEM image of the nBGs@Pt. (d) The EDX images of the element distribution: Pt, P, O, Ca. (e) The size distribution of the nBGs@Pt. (f) The zeta potential of nBGs and the nBGs@Pt. (g) The XRD spectrum of nBGs@Pt.
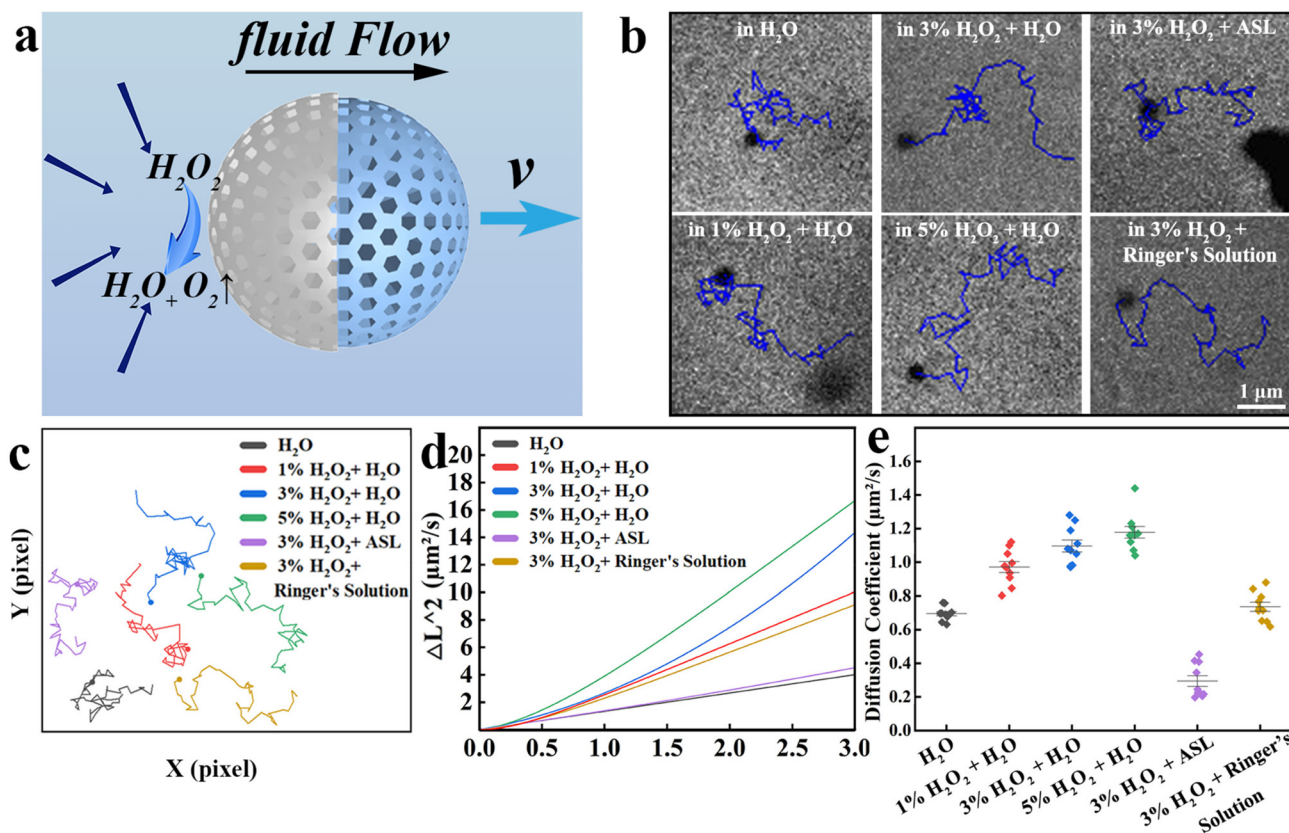
concentration of H_2O_2 diminished the motion capacity, meanwhile multiple nBGs@Pt get stuck with each other. Therefore, we considered that the nBGs@Pt could resist the outflow of the dentin tubule fluid and enter the dentin tubule. Due to the limited light transmission of teeth, there is no suitable microscope system for the study of dentin tubules. However, polycarbonate films are similar in structure to dentin, and both have microchannels with an average diameter of 3 μm, which suggests they can be used as a model for relevant research. We therefore chose polycarbonate films to simulate dentin tubules and evaluated the treatment effect with real teeth in *in vivo* studies. The video of the nanomotors entering the tubules was also successfully photographed, as shown in Fig. S2, S3 and Video S3.†

3.3 *In vivo* and *in vitro* toxicity tests

After treatment, the nBGs@Pt were stuck in the dentinal tubules. Next, we tested the toxicity of the nBGs@Pt to HGFs and mice. Fig. 3a shows the cell viability after incubation with

1, 0.5, 0.25, 0.125, 0.1 mg mL^{-1} concentration of the nBGs@Pt for 48 h, where the cell viability was found to be 105.69%, 115.96%, 103.47%, 106.61%, and 95.32%, respectively, showing no statistical significance compared with the control. Fig. 3b shows the LIVE/DEAD staining images of HGFs after adding different concentrations of the nBGs@Pt, which showed good safety. The results indicated that nBGs@Pt at 1 mg mL^{-1} or a lower concentration were safe enough for HGFs.

Then the mice were intragastrically administered with 1 mg mL^{-1} nBGs@Pt. Fig. S4† shows the weight change of the mice after the intragastric administration. No significant weight loss occurred in either group. This proved that no acute poisoning had occurred. For further study, we collected arterial blood from two groups of mice for routine blood tests. The results are shown in Fig. 3c. We conducted a statistical analysis of these data and found no significant difference between the two groups. Finally, the vital organs of the mice were collected and H&E staining was performed (Fig. 3d). There was no sig-

Fig. 2 The motion behaviors analysis of the nBGs@Pt JANUS nanomotor. (a) The characterization of the propulsion of nBGs@Pt Janus nanomotors. (b) The motion trajectory of nBGs@Pt in different situations. (c) The trajectory diagram analysis of nBGs@Pt in different situations. (d) MSD of nBGs@Pt in different situations. (e) The diffusion coefficient of nBGs@Pt in different situations.

nificant histological change found. These results proved that a 1 mg mL^{-1} concentration of nBGs@Pt is safe enough, and thus this was adopted in the following study.

3.4 *Ex vivo* dentin disks blocking and remineralization of the dentinal tubules

First, we incubated nBGs or nBGs@Pt with ASL to observe the formation of HA. The final products of the nBGs are shown in Fig. S5.† The XRD results showed the characteristic peaks of HA at $\theta = 26°$, 32°, 39°, 46°, 49°, and 53°. These peaks corresponded to the crystallinity of HA (PDF#00-055-0592), proving that the nBGs had a good HA-formation ability. Fig. 4a shows a SEM image of the final product of the nBGs@Pt incubation with ASL after 1, 4, 7 d, where it can be seen that the amount of scaly substance increased over time. The same phenomenon was observed in the nBGs, as shown in Fig. S5a.† The amount of scaly substance was more abundant than for the nBGs@Pt. Then we performed XRD tests and as shown in Fig. 4b, new peaks appeared at $\theta = 26°$, 32°, 49°, and 53°, but these were much shorter than in Fig. S5b.† No peaks appeared at 39° and 46° because they were obscured by the peaks of Pt. These results prove that the Pt coated layer has little effect on the formation of HA and the nBGs@Pt also showed a good HA-formation ability.

When dentin hypersensitivity strikes, all affected teeth are vital pulp and have a certain pressure in the pulp cavity. Meanwhile, dentin tubules are filled with dentin fluid, which drains constantly due to pressure in the pulp cavity. To investigate the entry effect of the nanomotors in this situation, we chose hydraulic pressure to simulate the pressure in the pulp cavity and Ringer's solution to simulate dentin fluid based on a previous study.[37,39] The pressure model is shown in Fig. 4c. The dentin sensitivity models were constructed by etching with EDTA. Fig. S6a and b† show the transverse and longitudinal sections of dentin tubules in the dentin sensitivity model. Those models were treated 1 or 3 times with nBGs and nBGs@Pt, respectively.

Then, we studied the entry and blocking effect of dentin tubules after 1 or 3 treatments by nBGs or nBGs@Pt, respectively. Fig. 4d shows the typical SEM image of 1 treatment by nBGs or nBGs@Pt. Both sets of tubules remained empty, which we considered was due to the low particle content. Compared with nBGs, nBGs@Pt were more located in tubules than around the tubules, which verified that the automatic motion ability of nBGs@Pt was effective for entering the tubules. After 3 treatments, the results in Fig. 4e were more obvious, whereby in the nBGs@Pt model, most dentin tubules were filled with nanomotors and a few nanomotors were dis-
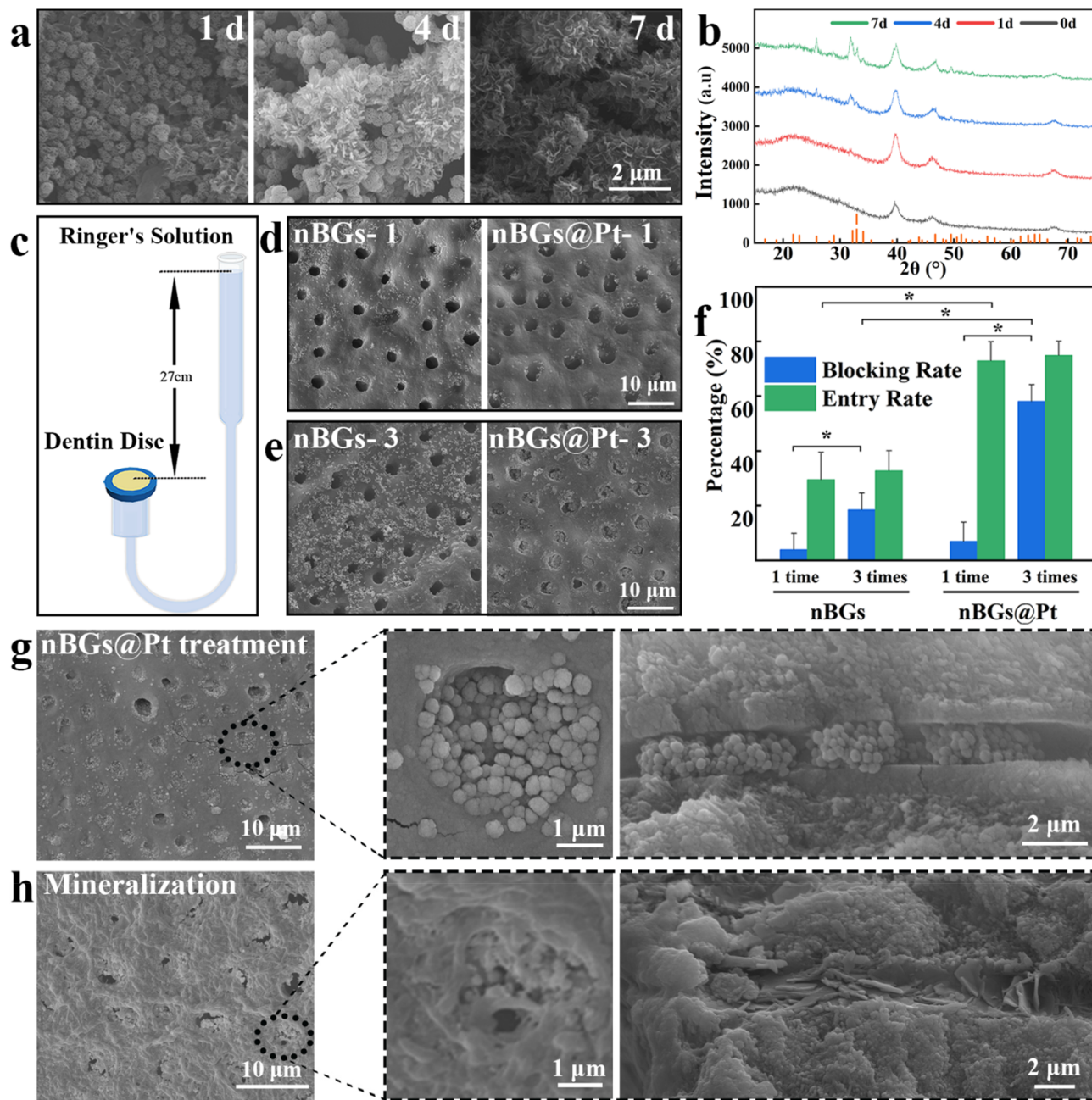
Fig. 3 The iosecurity test of the nBGs@Pt JANUS nanomotor. (a) The cell cytotoxicity test of nBGs@Pt in different concentrations. (b) Gingival fibroblast dead and alive staining. (c) The lood routine index: white blood cells, lymphocytes, monocytes, neutrophilic granulocyte percentage, hemoglobin, red blood cells, hematocrit, blood platelets, comparison of nBGs@Pt with a control. (d) The HE staining of important organs of mice; comparison of nBGs@Pt with a control.

tributed around compared with the nBGs. We also consider that the number of nanomotors also play an important role in tubules blocking.

In order to quantify the blocking of dentin disks, we counted the particles after 1 or 3 times treatment respectively (Fig. 4f). After 1 treatment, the blocking rate of the nBGs@Pt (6.88%) was higher than for the nBGs (3.86%). The blocking rate of both groups was still very low due to the low quantity of particles. The entry rate of the nBGs@Pt (72.97%) exhibited a statistically significant two-fold increase compared to that of the nBGs (29.53%), which was attributed to the automatic motion function. After 3 treatments, the blocking rate increased for both significantly, whereby the nBGs@Pt reached 58% and nBGs reached 18%, with statistical differences between and within the groups. This result confirmed the previous hypothesis about quantity. The entry rate of the nBGs@Pt (74.95%) was still more than twice as large as nBGs (32.72%). Remarkably, the entry rate of the two groups showed little increase with no significant statistical difference. These results suggest that the nBGs@Pt was able to resist fluid outflow and could enter into the tubes without being flushed out. Based on previous research,[40] in the sensitivity-occurring zone, 75% of the dentinal tubules were open, whereas in this study our blocking rate reached 58.05%, which means it is still able to meet the treatment.

Next, we studied the remineralization of nBGs@Pt to dentin disks. The dentin disks treated by nBGs@Pt 3 times were incubated with ASL for 7 d. Fig. 4g shows the morphology of the dentin surface after treatment by nBGs@Pt three times, where it can be seen that the dentinal tubules were full of nBGs@Pt in both the longitudinal and cross-sectional images. The important role played by the automatic movement ability of nBGs@Pt was further verified. Fig. 4h shows the morphology of the dentin surface after remineralization. After incubation, most space was filled with HA, and it was hard to distinguish the morphology of the dentin tubules. As shown in Fig. S7a,† all the tubules were filled with HA, and the longitudinal section shows that the interior was also filled by HA (Fig. S7b†). We analyzed the SEM images of the dentin disks after remineralization by image J, counted the area of the blocked regions, and then calculated the percentage blocking area over the whole image, and found that the blocking rate could reach 96.07% (Fig. S7c†). The results proved that both nBGs@Pt and HA formed by nBGs@Pt have good blocking effects on dentin tubules. We performed statistical analysis, respectively, and found the average penetrating depth of the

move it showed a better blocking and entry rate at the dentin disc in the pressure model. Through the observation of the longitudinal section, the deepest blocking depth of HA was more than 30 μm. In the ASL environment, the formation of HA could connect nanomotors with each other to fill gaps in the dentin tubules, isolate stimuli, and maintain long-term efficacy. In addition, bioglass has certain antibacterial properties,[41] thus preventing plaque formation and reducing the occurrence of caries or periodontal disease.

4. Conclusions

In this study, we successfully prepared a nBGs@Pt nanomotor for dentin hypersensitivity and achieved a good effect. The nBGs@Pt displayed a Janus structure with an average size of 290 nm. Pt as a catalyst promoted H_2O_2 to decompose, generating a concentration gradient, which provided power to make the nanomotors automatically move even in high viscosity media. The speed of the nanomotors in Ringer's solution could reach 1.0561 μm s^{-1}, which was strong enough to resist liquid outflow and allow them to enter tubules, and to obtain a high blocking rate and entry rate. The formation of HA could penetrate more than 10 μm into the dentin tubule and maintain long-term efficacy. The findings suggest our nanomotors solution may be a suitable mechanical resistant conservative treatment option for dentin hypersensitivity. In addition, the core of the nanomotors also has certain antibacterial abilities, promoting bone formation ability, which may have certain application value in the field of periodontal disease treatment.

Conflicts of interest

There are no conflicts to declare.

Ethical statement

Statement of human rights

All experiments were performed in compliance with the ethical standards laid down in "Declaration of Helsinki" (1964), "Ethical Review of Biomedical Research Involving Humans" (Health Commission of the People's Republic of China, 2022), "Opinions on Strengthening the Ethical Governance of Science and Technology" (Harbin Medical University, 2022-03-20).

All human body tissue experiments were approved by the Medical Ethics Committee of the Second Affiliated Hospital of Harbin Medical University (YJSKY2022-384).

Statement of animal rights

All experiments were performed in compliance with "Principles of Laboratory Animal Care" (NIH publication No. 85-23, revised 1985), "Regulations on the Administration of Laboratory Animals" (Order No. 2 of the State Science and Technology Commission of the People's Republic of China,

1988), "Administration of laboratory animal License" (Harbin Medical University, 2022-02-23).

All the animal experiments were approved by the Animal Ethics Committee of the Harbin Medical University, Harbin, China (SYDW2018-001), all laboratory mice were purchased from the animal experiment center of the Second Affiliated Hospital of Harbin Medical University.

Statement of informed consent

All the extracted teeth were obtained from the Second Affiliated Hospital of Harbin Medical University, all the patients were informed and agreed to provide extracted teeth.

References

1 M. Brannstrom, L. A. Linden and A. Astrom, *Caries Res.*, 1967, **1**, 310–317.
2 R. Orchardson and D. G. Gillam, *J. Am. Dent. Assoc.*, 2006, **137**(7), 990–998.
3 Y. C. Chiang, H. J. Chen, H. C. Liu, S. H. Kang, B. S. Lee, F. H. Lin, H. P. Lin and C. P. Lin, *J. Dent. Res.*, 2010, **89**, 236–240.
4 S. Tan, S. Chen, Y. Wang, F. Wu, Y. Shi, J. Wang, Y. Du and S. Zhang, *Dent. Mater.*, 2020, **36**, 816–825.
5 Z. Chen, Y. Duan, S. Shan, K. Sun, G. Wang, C. Shao, Z. Tang, Z. Xu, Y. Zhou, Z. Chen, R. Tang, H. Pan and Z. Xie, *Nanoscale*, 2022, **14**, 642–652.
6 L. C. Gerhardt and A. R. Boccaccini, *Materials*, 2010, **3**, 3867–3910.
7 N. Pinchuk, O. Parkhomey and O. Sych, *Nanoscale Res. Lett.*, 2017, **12**, 111.
8 Y. Niu, L. Guo, J. Liu, H. Shen, J. Su, X. An, B. Yu, J. Wei, J. W. Shin, H. Guo, F. Ji and D. He, *J. Mater. Chem. B*, 2015, **3**, 2962–2970.
9 B. S. Lee, H. Y. Tsai, Y. L. Tsai, W. H. Lan and C. P. Lin, *Dent. Mater. J.*, 2005, **24**, 562–569.
10 S. Chitra, R Chandran, R. Ramya, D. Durgalakshmi and S. Balakumar, *Biomed. Mater.*, 2022, **17**(3), 035001.
11 Y. E. Choe, Y. J. Kim, S. J. Jeon, J. Y. Ahn, J. H. Park, K. Dashnyam, N. Mandakhbayar, J. C. Knowles, H. W. Kim, S. K. Jun, J. H. Lee and H. H. Lee, *Dent. Mater.*, 2022, **38**, 363–375.
12 M. Erol-Taygun, K. Zheng and AR Boccaccini, *Int. J. Appl. Glass Sci.*, 2013, **4**, 136–148.
13 Y. Wang, T. Liao, M. Shi, C. Liu and X. Chen, *Mater. Lett.*, 2017, **206**, 205–209.

14 M. M. Moreira, L. R. R. da Silva, T. A. D. Mendes, S. L. Santiago, S. E. Mazzetto, D. Lomonaco and V. P. Feitosa, *Dent. Mater.*, 2018, **34**, 1144–1153.

15 B. Khezri and M. Pumera, *Adv. Mater.*, 2019, **31**(14), 1806530.

16 X. Ma, A. C. Hortelao, A. Miguel-Lopez and S. Sanchez, *J. Am. Chem. Soc.*, 2016, **138**, 13782–13785.

17 Y. Wang, Y. Liu, Y. Li, D. Xu, X. Pan, Y. Chen, D. Zhou, B. Wang, H. Feng and X. Ma, *Research*, 2020, **2020**, 7962024.

18 H. Zhou, C. C. Mayorga-Martinez, S. Pane, L. Zhang and M. Pumera, *Chem. Rev.*, 2021, **121**, 4999–5041.

19 R. Dong, Y. Hu, Y. Wu, W. Gao, B. Ren, Q. Wang and Y. Cai, *J. Am. Chem. Soc.*, 2017, **139**, 1722–1725.

20 C. C. Mayorga-Martinez, J. Zelenka, K. Klima, P. Mayorga-Burrezo, L. Hoang, T. Ruml and M. Pumera, *ACS Nano*, 2022, **16**, 8694–8703.

21 J. Katuri, X. Ma, M. M. Stanton and S. Sanchez, *Acc. Chem. Res.*, 2017, **50**, 2–11.

22 X. Ma and S. Sanchez, *Nanomedicine*, 2017, **12**, 1363–1367.

23 S. S. Tang, F. Y. Zhang, H. Gong, F. N. Wei, J. Zhuang, E. Karshalev, B. E. F. de Avila, C. Y. Huang, Z. D. Zhou, Z. X. Li, L. Yin, H. F. Dong, R. H. Fang, X. J. Zhang, L. F. Zhang and J. Wang, *Sci. Rob.*, 2020, **5**(43), eaba6137.

24 B. Wang, K. F. Chan, K. Yuan, Q. Q. Wang, X. F. Xia, L. D. Yang, H. Ko, Y. X. J. Wang, J. J. Y. Sung, P. W. Y. Chiu and L. Zhang, *Sci. Rob.*, 2021, **6**(52), abd2813.

25 X. Liu, X. Sun, Y. Peng, Y. Wang, D. Xu, W. Chen, W. Wang, X. Yan and X. Ma, *ACS Nano*, 2022, **16**, 14666–14678.

26 W. Chen, H. Zhou, B. Zhang, Q. Cao, B. Wang and X. Ma, *Adv. Funct. Mater.*, 2022, **32**(18), 2110625.

27 H. Liang, F. Peng and Y. Tu, *Nanoscale*, 2023, **15**, 953–962.

28 X. Ma, A. C. Hortelao, T. Patino and S. Sanchez, *ACS Nano*, 2016, **10**, 9111–9122.

29 A. M. Pourrahimi and M. Pumera, *Nanoscale*, 2018, **10**, 16398–16415.

30 J. Shao, S. Cao, H. Che, M. T. De Martino, H. Wu, L. Abdelmohsen and J. C. M. van Hest, *J. Am. Chem. Soc.*, 2022, **144**, 11246–11252.

31 H. Khosropanah, F. Koohpeima, F. Ieal and F. Yazid, *J. Dent.*, 2012, **13**, 44–48.

32 X. Du, C. Zhao, Y. Luan, C. Zhang, M. Jaroniec, H. Huang, X. Zhang and S. Z. Qiao, *J. Mater. Chem. A*, 2017, **5**, 21560.

33 J. R. Howse, R. A. Jones, A. J. Ryan, T. Gough, R. Vafabakhsh and R. Golestanian, *Phys. Rev. Lett.*, 2007, **99**, 048102.

34 Y. Choi, W. Sun, Y. Kim, I. R. Kim, M. K. Gong, S. Y. Yoon, M. K. Bae, B. S. Park, S. B. Park and Y. I. Kim, *Nanomaterials*, 2020, **10**, 1943.

35 H. H. Chang, C. L. Yeh, Y. L. Wang, G. W. Liu, H. P. Lin and C. P. Lin, *J. Formosan Med. Assoc.*, 2020, **119**, 1835–1841.

36 M. Xuereb, P. Vella, D. Damidot, C. V. Sammut and J. Camilleri, *J Endod.*, 2015, **41**, 111–124.

37 N. Chinajitphan, E. Chunhacheevachaloke and O. Ajcharanukul, *Arch. Oral Biol.*, 2019, **99**, 58–65.

38 B. Ciucchi, S. Bouillaguet, J. Holz and D. Pashley, *J Endod.*, 1995, **21**, 191–194.

39 P. Charoenlarp, S. Wanachantararak, N. Vongsavan and B. Matthews, *Arch. Oral Biol.*, 2007, **52**, 625–631.

40 M. Yoshiyama, Y. Noiri, K. Ozaki, A. Uchida, Y. Ishikawa and H. Ishida, *J Dent Res.*, 1990, **68**, 1293–1297.

41 D. Khvostenko, T. J. Hilton, J. L. Ferracane, J. C. Mitchell and J. J. Kruzic, *Dent. Mater.*, 2016, **32**, 73–81.